MNRAS **449,** 2845–2852 (2015) doi:10.1093/mnras/stv497

Constraining the growth of perturbations with lensing of supernovae

Luca Amendola,[1] Tiago Castro,[2] Valerio Marra[2,3]⋆ and Miguel Quartin[2]

[1]*Institut für Theoretische Physik, Universität Heidelberg, Philosophenweg 16, D-69120 Heidelberg, Germany*
[2]*Instituto de Física, Universidade Federal do Rio de Janeiro, CEP 21941-972 Rio de Janeiro, RJ, Brazil*
[3]*Departamento de Física, Universidade Federal do Espírito Santo, 29075-910 Vitória, ES, Brazil*

Accepted 2015 March 4. Received 2015 February 17; in original form 2014 December 16

ABSTRACT

A recently proposed technique allows one to constrain both the background and perturbation cosmological parameters through the distribution function of Type Ia supernova apparent magnitudes. Here we extend this technique to alternative cosmological scenarios, in which the growth of structure does not follow the Λ cold dark matter prescription. We apply the method first to the supernova data provided by the JLA catalogue combined with all the current independent redshift distortion data and with low-redshift cluster data from *Chandra* and show that although the supernovae alone are not very constraining, they help in reducing the confidence regions. Then we apply our method to future data from Large Synoptic Survey Telescope (LSST) and from a survey that approximates the *Euclid* satellite mission. In this case we show that the combined data are nicely complementary and can constrain the normalization σ_8 and the growth rate index γ to within 0.6 per cent and 7 per cent, respectively. In particular, the LSST supernova catalogue is forecast to give the constraint $\gamma(\sigma_8/0.83)^{6.7} = 0.55 \pm 0.1$. We also report on constraints relative to a step-wise parametrization of the growth rate of structures. These results show that supernova lensing serves as a good cross-check on the measurement of perturbation parameters from more standard techniques.

Key words: gravitational lensing: weak – supernovae: general – cosmological parameters – cosmology: observations – large-scale structure of Universe.

1 INTRODUCTION

The need to understand the nature of the mechanism that accelerates the Universe expansion is driving several new observational campaigns. Dedicated surveys like the Dark Energy Survey or satellites like *Euclid*, along with several other ground-based surveys, will soon generate very large data bases of galaxy redshifts and images and of supernova (SN) light curves, all of them containing information of cosmological dynamics.

In this paper, following a series of previous works (Marra, Quartin & Amendola 2013; Castro & Quartin 2014; Quartin, Marra & Amendola 2014), we exploit a complementary method based on lensing of distant Type supernovae (SNe Ia). The idea behind our approach is rather simple. The apparent magnitude of standard candles depends on both the background cosmology and the gravitational perturbations crossed by the photons along their path; by analysing the statistical distribution of the SN Ia apparent magnitudes around their mean value, we can infer the properties of the intervening matter perturbations. This follows ideas first discussed in Bernardeau, Van Waerbeke & Mellier (1997), Hamana & Futamase (2000), Valageas (2000) and later further developed in Dodelson & Vallinotto (2006). In practice, some assumptions on the intrinsic scatter of SNe Ia are required; in particular, we assume that the intrinsic scatter is independent of redshift, since this was shown to be the most reasonable hypothesis using Bayesian analysis (Castro & Quartin 2014) and also agrees with the underlying motivation for using SNe Ia as standard candles whose properties do not depend on distance.

As mentioned earlier, SN lensing depends both on background and perturbation parameters. Building *N*-body simulations for a reasonable grid of cosmological parameters and then extracting the theoretical magnitude distribution is hardly feasible. To circumvent this limitation we employed realizations of the perturbed universe using the TURBOGL[1] implementation of SGL (stochastic Gravitational Lensing) – a very fast method developed by Kainulainen & Marra (2009, 2011a,b) – whose results are in concordance with recent *N*-body simulations but orders of magnitude faster (Marra et al. 2013). They are also in very good agreement with observational data (Jönsson et al. 2010a,b; Kronborg et al. 2010) and with other recent independent theoretical estimations (Ben-Dayan et al. 2013).

⋆ E-mail: valerio.marra@me.com

[1] The work carried out in this paper is based on (the latest) version 3.0 of TURBOGL available at turbogl.org.

In our previous papers we discussed how the SN Ia magnitude scatter can be employed to constrain cosmological parameters within the standard model of cosmology. In a Λ cold dark matter (ΛCDM) scenario it was confirmed that the matter density $\Omega_{\rm m0}$ and the amplitude of the power spectrum σ_8 were the most important cosmological parameters as far as SN lensing is concerned. As the former is tightly constrained by the SN magnitudes themselves (i.e. by the first moment of the distribution), the most important *new* information gained was the value of σ_8. In this respect, we found that while present catalogues start to have the statistical power to make the first measurement of σ_8 (Castro & Quartin 2014), Large Synoptic Survey Telescope (LSST) will be able to constrain the amplitude of the power spectrum at the level of a few per cent with SNe only (Quartin et al. 2014).

Here we extend our previous analysis to the case of a non-standard growth rate, which we model using either the $f_{\rm g} \approx \Omega_{\rm m}(z)^{\gamma}$ or the step-wise $f_{\rm g} = f_i$ parametrization. We then apply the Method-of-Moments (MeMo; see Quartin et al. 2014) – which basically compares the observed central moments of the magnitude distribution to the theoretical predictions – to current and future SN catalogues. Regarding the latter we base our study on the LSST (see Abell et al. 2009) and the *Wide-Field Infrared Survey Telescope* (*WFIRST*; see Green et al. 2012). Regarding current data, we use the most recent SN catalouge dubbed JLA (acronym for Joint Lightcurve Analysis; see Betoule et al. 2014).

In order to illustrate the complementarity of our method, we combine the current results on σ_8 and γ with low-redshift cluster data from *Chandra* (see Vikhlinin et al. 2009) and with redshift distortion data from all the current independent surveys: 2dFGS, 6dFGS, LRG, BOSS, CMASS, WiggleZ and VIPERS (see respectively, Percival et al. 2004; Beutler et al. 2012; Samushia, Percival & Raccanelli 2012; Chuang & Wang 2013; Tojeiro et al. 2012; Beutler et al. 2014; Reid et al. 2014; Samushia et al. 2014; Blake et al. 2012 and de la Torre et al. 2013); and our forecast results with constraints from a survey that approximates the *Euclid* satellite mission (see Laureijs et al. 2011; Amendola et al. 2013).

It is clear that the large increase in SN statistics provided by the LSST should be accompanied by a similar increase on our understanding of the various SN systematics. In fact in the past few years a large effort has been devoted to testing and improving the calibration of SN Ia and to correcting their light curves in order to understand and control systematics (Kessler et al. 2009; Conley et al. 2011; Betoule et al. 2013; Scolnic et al. 2014). In the forecasts presented here, we assume that systematics can be kept subdominant even for LSST, but it is not at all clear if this will be achieved.

This paper is organized as follows. In Section 2, we will state the adopted model for background and perturbations, and also the method we use to compute the lensing distribution. In Section 3, we will build the likelihood functions for the various observables and the corresponding data, while in Section 4 we will show the constraining power of SN catalouges. Conclusions are drawn in Section 5. Finally, in Appendix A simple fits for the lensing moments as a function of $\{z, \sigma_8, \gamma\}$ will be given.

2 MODEL

2.1 Matter and lensing model

We will obtain the lensing probability density function (PDF) for the desired model parameters using the TURBOGL code, which is the numerical implementation of the SGL method introduced in Kainulainen & Marra (2009, 2011a,b). The SGL method is based on (i) the weak-lensing approximation and (ii) generating stochastic configurations of inhomogeneities along the line of sight.

Regarding (ii), the matter density contrast $\delta_{\rm M}(r, t)$ is modelled in this paper as a random collection of Navarro–Frenk–White (NFW) haloes, whose abundance is calculated using the halo mass function given in Courtin et al. (2011) [basically a refitted Sheth & Tormen (1999) mass function] and whose concentration parameters (which depend on cosmology) are calculated using the universal and accurate model proposed in Zhao et al. (2009). Linear correlations in the halo positions are neglected by the SGL method: this should be indeed a good approximation as the contribution of the two-halo term is negligible with respect to the contribution of the one-halo term (Kainulainen & Marra 2011b). Overall, the modelling was proved (Marra et al. 2013) to be accurate for the redshift range of $z \lesssim 1.5$ in which we are mainly interested in this paper. At higher redshifts the relative importance of unvirialized objects such as filaments becomes more important and one may need to include them in the modelling (Kainulainen & Marra 2011a).

Regarding (i), the lens convergence κ in the weak-lensing approximation is given by the following line-of-sight integral (Bartelmann & Schneider 2001):

$$\kappa(z_{\rm s}) = \rho_{\rm MC} \int_0^{r_{\rm s}} {\rm d}r\, \mathcal{G}(r, r_{\rm s})\, \delta_{\rm M}(r, t(r))\,, \tag{1}$$

where the quantity $\delta_{\rm M}(r, t)$ is the local matter density contrast (which is modelled as described above), $\rho_{\rm MC} \equiv a_0^3\, \rho_{\rm M0}$ is the constant matter density in a comoving volume, and the function

$$\mathcal{G}(r, r_{\rm s}) = \frac{4\pi G}{c^2\, a}\, \frac{r(r_{\rm s} - r)}{r_{\rm s}}$$

gives the optical weight of a matter structure at the comoving radius r (assuming spatial flatness). The functions $a(t)$ and $t(r)$ are the scale factor and geodesic time for the background Friedmann-Lemaître-Robertson-Walker (FLRW) model, and $r_{\rm s} = r(z_{\rm s})$ is the comoving position of the source at redshift $z_{\rm s}$. At the linear level, the shift in the distance modulus caused by lensing is expressed in terms of the convergence only:

$$\Delta m(z) \simeq -\frac{5}{\log 10}\, \kappa(z)\,. \tag{2}$$

Equation (1) connects the statistics of the matter distribution to the statistics of the convergence distribution: by studying the latter one can gain information on the former and thus on the nature of dark energy. The SGL method for computing the lens convergence is based on generating random configurations of haloes along the line of sight and computing the associated integral in equation (1) by binning into a number of independent lens planes. A detailed explanation of the SGL method can be found in Kainulainen & Marra (2009, 2011a,b).

Because of theoretical approximations and modelling uncertainties, the TURBOGL code can be relied upon at the level of $\sim$10 per cent as far as the moments of the lensing PDF are concerned (Marra et al. 2013).

2.2 Growth of perturbations

In this paper, we aim at testing with SN data the growth of perturbations. We will take a minimal and simple approach: we will assume that the background evolves according to the standard ΛCDM model but that matter perturbations grow according to a different theory. This is actually the case for most of the viable $f(R)$ and scalar-field models (Amendola & Tsujikawa 2010). Therefore,

while the SN Hubble diagram in each redshift bin will have its *mean* unchanged, it will feature a different *dispersion* due to a different lensing caused by a different growth of structures.

In this section, we will discuss two ways to parameterize the growth rate of perturbations. Before starting, however, we would like to point out that we will use a halo mass function and concentration parameter model (see Section 2.1) which have been tested within the standard paradigm. Therefore, our results may suffer from systematic errors when inspected far from the fiducial model, which we take to be the *Planck* 2013 best fitted to observations of the cosmic microwave background (CMB) and baryon acoustic oscillations (BAO; Planck Collaboration XVI 2014, table 5).

2.2.1 γ-parametrization

The linear growth of matter perturbations is described by the growth function $G(z)$, usually normalized to unity at the present time, $G(0) = 1$. It is useful to describe the growth of perturbations via the growth rate $f_{\rm g}$, which is the logarithmic derivative of the growth function with respect to the scale factor $a = 1/(1+z)$:

$$f_{\rm g} \equiv -\frac{{\rm d}\ln G}{{\rm d}\ln(1+z)} \approx \Omega_{\rm m}(z)^{\gamma} \,. \tag{3}$$

The last equation approximates the growth rate as a power of $\Omega_{\rm m}(z) = \Omega_{\rm m0}(1+z)^3/E^2(z)$, where $E(z) = H(z)/H_0$, H is the Hubble parameter and the subscript '0' denotes the present-day value of a quantity. Within General Relativity (GR) and for the ΛCDM model $f_{\rm g}$ is accurately described by equation (3) with $\gamma = \gamma_{\rm sm} \approx 0.55$ (Amendola & Tsujikawa 2010), and the subject of Section 4 will be to understand how strongly can lensing of SNe constrain γ around this standard value. Indeed, any measured deviation from $\gamma_{\rm sm}$ will signal the demise of the standard model of cosmology.

The growth function is obtained by the following integral of the growth rate:

$$G(z) \,=\, \exp\left(-\int_0^z \frac{{\rm d}\bar{z}}{1+\bar{z}} f_{\rm g}(\bar{z})\right) . \tag{4}$$

In the Einstein–de Sitter (EdS) model – which is effectively the same as ΛCDM at $1 \ll z \ll 1000$ – one has $f_{\rm g} = 1$ and $G_{\rm EdS} = 1/(1+z)$.

2.2.2 f-*parametrization*

The parametrization of equation (3), while certainly convenient, has a constrained redshift evolution and one may wish for a more general non-parametric description of the growth rate at the various redshifts. One possibility is to model the growth rate as a step-wise function (Amendola et al. 2013):

$$f_{\rm g} = f_i \,, \tag{5}$$

where f_i is the value of the growth rate in the redshift bin $[z_{i-1}, z_i)$, where $z_0 = 0$ and $i = 1, \ldots, n$. We will use bins of width $\Delta z = 0.2$, which allows for a reconstruction – with negligible error – of the standard model growth function $G(z)$. The fiducial values of f_i are given in Table 1.

Table 1. Fiducial values of $f_{1,\ldots,5}$ of equation (5), corresponding to $\Omega_{\rm m}(z)^{\gamma_{\rm sm}}$ calculated at the centre of each redshift bin.

$[z_{i-1}, z_i)$	[0, 0.2)	[0.2, 0.4)	[0.4, 0.6)	[0.6, 0.8)	[0.8, 1.0)
f_i	0.58	0.68	0.76	0.81	0.86

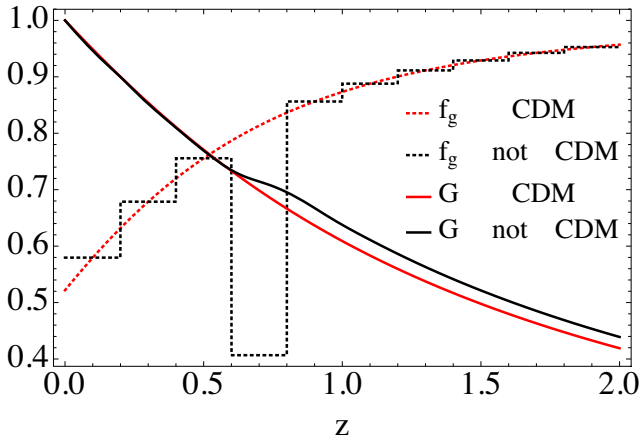

Figure 1. Growth function $G(z)$ and growth rate $f_{\rm g}(z)$ for the ΛCDM model (red) and a model whose growth rate is parametrized according to a step-wise function (black) which has the standard value for every redshift bin except the bin [0.6, 0.8) where $f_{\rm g}$ has half its standard value. See Section 2.2.2 for more details.

The growth function, obtained performing the integral of equation (4), is then

$$G(z) = \left(\frac{1+z}{1+z_{\bar{n}}}\right)^{-f_{\bar{n}+1}} \prod_{i=1}^{\bar{n}} \left(\frac{1+z_i}{1+z_{i-1}}\right)^{-f_i} , \tag{6}$$

where $\bar{n}$ is such that $z_{\bar{n}} < z$.

In Fig. 1 an example of a step-wise growth rate and corresponding growth function are shown. Note that the non-standard G is higher in the past for an $f_{\rm g}$ which is lower than in the ΛCDM in a low-z bin because G is normalized to unity at present time.

It is worth stressing that the main feature of this parametrization is its flexibility. It allows our discussion to be very broad, and if one intends to test any modified gravity theory with the analysis developed here one needs only to derive the values of the $\{f_i\}$ set for the chosen theory and update the fiducial Table 1.

3 METHOD AND DATA

3.1 SN data

3.1.1 *Method-of-Moments*

Here we summarize the so-called Method-of-Moments (MeMo). Originally discussed in Quartin et al. (2014) in the context of forecasts, the MeMo has recently passed its first test with real data as shown in Castro & Quartin (2014). In a nutshell, the idea is to use the scatter in the Hubble diagram to measure cosmological parameters on which gravitational lensing depends: $\Omega_{\rm m0}$ and σ_8 in Quartin et al. (2014), Castro & Quartin (2014) and also γ or f_i in this work. The MeMo approach is basically a χ^2 approach where we measure the mean μ_1' (which is independent of lensing due to photon number conservation) and the first three central moments $\{\mu_2, \mu_3, \mu_4\}$ (which we will collectively refer to simply as μ_{1-4}) and compare them with the corresponding theoretical predictions. The latter is computed through the convolution of the lensing PDF ($\mu_{1-4,\rm lens}$, see Section 2.1) with the intrinsic SN dispersion distribution ($\{\sigma_{\rm int}, \mu_{3,\rm int}, \mu_{4,\rm int}\}$, which we define including all instrumental noise contributions). The final relation between those quantities are given by (Quartin et al. 2014)

$$\mu_2 \;\equiv\; \sigma^2_{\rm tot} \;=\; \sigma^2_{\rm lens} + \sigma^2_{\rm int} \,, \tag{7}$$

$$\mu_3 = \mu_{3,\rm lens} + \mu_{3,\rm int}\,, \tag{8}$$

$$\mu_4 = \mu_{4,\rm lens} + 6\,\sigma^2_{\rm lens}\,\sigma^2_{\rm int} + 3\,\sigma^4_{\rm int} + \mu_{4,\rm int}\,. \tag{9}$$

Although the number of moments to be used in the analysis is in principle arbitrary as each new moment adds more information, it was shown in Quartin et al. (2014) that for SN analyses basically all the information is already contained in the first four moments μ_{1-4} (and a very good fraction of it already in μ_{1-3}).

The full MeMo likelihood is then

$$L_{\rm MeMo}({\rm Data}|\Theta_{\rm cosmo}) = \exp\left(-\frac{1}{2}\sum_j^{\rm bins}\chi^2_j\right), \tag{10}$$

$$\chi^2_j = \left(\boldsymbol{\mu} - \boldsymbol{\mu}_{\rm data}\right)^t\ \Sigma_j^{-1}\ \left(\boldsymbol{\mu} - \boldsymbol{\mu}_{\rm data}\right), \tag{11}$$

$$\boldsymbol{\mu} = \{\mu_1',\ \mu_2,\ \mu_3,\ \mu_4\}, \tag{12}$$

where the vector $\boldsymbol{\mu}$ depends on the cosmological parameters ($\Theta_{\rm cosmo}$), and its second-to-fourth components are defined in equations (7)–(9). The mean μ_1' is the theoretical distance modulus. The components of the vector $\boldsymbol{\mu}_{\rm data}(z_j)$ are the moments inferred from the data, which for the forecasts we take to be $\boldsymbol{\mu}(\Theta_{\rm cosmo})$ evaluated at the fiducial model and at redshift z_j. The covariance matrix Σ is also built using the fiducial moments and therefore does not depend explicitly on cosmology (but it does on z – see Quartin et al. 2014 for more details).

Even though the (most recent) JLA SN catalouge (Betoule et al. 2014) showed no need of intrinsic moments higher than the second (Castro & Quartin 2014), with more accurate and precise surveys new systematic effects may become evident. Therefore, in order to obtain conservative results we allow the intrinsic SN distribution to also have non-zero intrinsic third ($\mu_{3,\rm int}$) and fourth ($\mu_{4,\rm int}$) moment. In the case of the JLA catalouge the statistics are not good enough to warrant $\mu_{4,\rm int}$ (Castro & Quartin 2014), but we keep it in the forecast analysis. Also, as in Castro & Quartin (2014) here we assume an intrinsic distribution constant in redshift since this was shown to be currently the most reasonable hypothesis using Bayesian analysis.

3.1.2 *SN catalouges*

In this section we describe the main details of the real and synthetic catalouges which we will use throughout this paper. We base our study on two future surveys – the LSST (see Abell et al. 2009) and the *WFIRST* (see Green et al. 2012) – and the most recent SN catalouge dubbed JLA (see Betoule et al. 2014).

LSST is an upcoming photometric survey currently in the design and development phase and expected to be operational between the end of this decade and the beginning of the next. By the end of its 10-year mission the number of SNe observed will be a few millions. This number includes all the expected observed SNe but in this paper we adopt the distribution based on the selection cut of signal to noise higher than 15 in at least two filters. With that cut the total number of SNe decreases to half a million in five years, and this was the number used here when computing the SN distribution shown in Fig. 2 (we include SN from both its 'main' and 'deep' surveys). The dispersion in the Hubble diagram of the LSST SN catalouge is not yet completely understood, but according to recent photometric surveys and rough estimations in the LSST white paper, it seems that a dispersion of 0.15 mag constant in redshift may be a reasonable hypothesis. Note that since we define $\sigma_{\rm int}$ to include noise, it corresponds to what is sometimes referred to as the total Hubble diagram dispersion (as opposed to the idealized intrinsic SN dispersion, not accounting for photometric redshift and other instrumental errors).

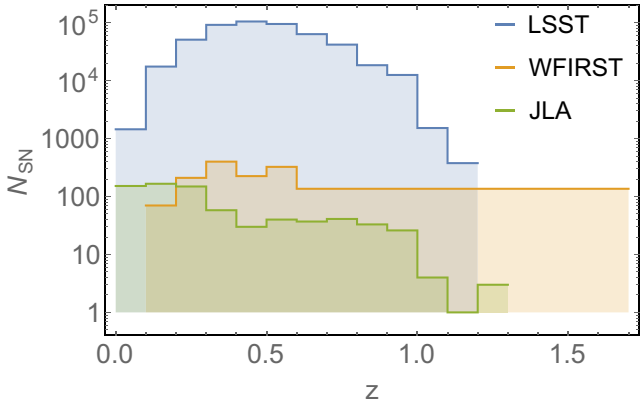

Figure 2. Observed SN redshift distributions of the JLA data set of 740 SNe and forecast distributions for LSST (5 years of observations for a total of 500 000 SNe, although this depend on the imposed quality cuts) and *WFIRST* (2700 SNe). See Section 3.1.2 for more details.

The other forecast used in this paper is *WFIRST*, a spectroscopic survey from NASA and its spectroscopy in the near-infrared can potentially reduce the intrinsic dispersion in the Hubble diagram to around 0.11 mag (which we will again assume constant in redshift) and achieve very deep redshifts as shown in the distribution of 2700 SNe plotted in Fig. 2. A similar proposal to *WFIRST* is DESIRE (Astier et al. 2014), which has a good overlap in redshift with *WFIRST* and seems to naturally complement LSST at higher redshifts. Here, however, we will consider only LSST and *WFIRST* as they are good representatives of future surveys.

The JLA catalouge, on the other hand, is a joint analysis of the 740 spectroscopically confirmed SN Ia of the SuperNova Legacy Survey (SNLS) and Sloan Digital Sky Survey (SDSS)-II collaboration. The redshift depth reaches the value of 1.3, but for redshifts higher than unity the number of SNe is insufficient to carry out the MeMo analysis. Here we use the same technical choices of Castro & Quartin (2014), which are bins of 0.1 width in redshift in the range $0 < z < 0.9$, yielding a total of 706 SNe.

3.2 *Chandra* low-redshift cluster sample

Chandra observations put tight constraints on $\Omega_{\rm m0}$ and σ_8 (Vikhlinin et al. 2009). Here we will focus on the low-redshift cluster sample which has a median redshift of $z \approx \bar{z} \equiv 0.05$. The posterior on $\Omega_{\rm m0}$ and σ_8 is given in Fig. 3 of Vikhlinin et al. (2009)[2] and can be approximated by the following binormal distribution:

$$L_{\rm cl} = L_{\rm cl,0}\,\exp\left[-\frac{1}{2}(\boldsymbol{x}-\boldsymbol{x}_{\rm bf})^t\,\Sigma_{\rm cl}^{-1}(\boldsymbol{x}-\boldsymbol{x}_{\rm bf})\right],$$

$$\boldsymbol{x} = \{\Omega_{\rm m0}, \sigma_8\}\,, \tag{13}$$

where $\Sigma_{\rm cl}$ is the covariance matrix (inverse of the Fisher matrix) which is determined by the dispersions $\sigma_{\Omega_{\rm m0}} = 0.05$ and $\sigma_{\sigma_8} = 0.08$ and the correlation $\rho = -0.985$. The best-fitting values are $\boldsymbol{x}_{\rm bf} = \{0.258, 0.8\}$. Also, we do not put prior constraints on $\Omega_{\rm m0}$ as the

[2] This figure includes also the high-redshift sample. However, the constraints are dominated by the low-redshift sample.

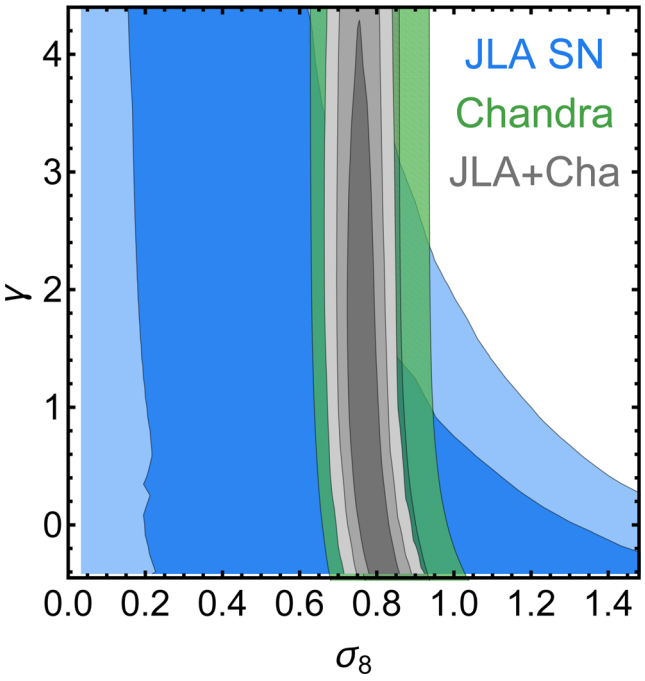

Figure 3. 1σ and 2σ marginalized constraints on γ and σ_8 for the JLA SN catalouge and the *Chandra* low-z cluster data. The combined contours are only capable of constraining σ_8, and just add very loose bounds on γ. See Section 4.1 for more details and Table 2 for the marginalized constraints.

latter will be already well constrained by SN data. Although this is an approximation to the posterior in Vikhlinin et al. (2009), it suffices for our scope which is to show the complementarity of SN lensing (using the JLA catalouge in this case) to other probes of matter perturbations.

As the latter constraints on Ω_{m0} and σ_8 are basically at present time ($\bar{z} \ll 1$), they depend weakly on the value of γ. To nevertheless account for such dependence we can proceed as follows. The constraint of equation (13) is obtained at $\bar{z}$, and then evolved to $z = 0$ using linear theory for $\gamma = \gamma_{sm}$. In order to expand this likelihood into the $\{\Omega_{m0}, \sigma_8, \gamma\}$ parameter space we have to evolve it back to $\bar{z}$ and then evolve it forward again to $z = 0$ using the growth function specific to the wanted γ. This simply means that for each slice of $\gamma = \text{const}$ one has to deform equation (13) according to

$$\sigma_{8,\gamma} = \frac{G_{\gamma_{sm}}(\bar{z})}{G_{\gamma}(\bar{z})}\,\sigma_8\,, \tag{14}$$

where G is given in equation (4) and also depends on the value of Ω_{m0}.

3.3 Growth rate data

Growth rate data measure the quantity $d = f(z)\sigma_8(z) = f(z)\sigma_8 G(z)$, which depends on the three parameters Ω_{m0}, γ, and σ_8, as seen in equations (3) and (4). One can then build the following likelihood function:

$$L_{gr} = L_{gr,0}\,\exp\left[-\frac{1}{2}(d_i - t_i)C_{ij}^{-1}(d_j - t_j)\right]\,, \tag{15}$$

where C_{ij} is the covariance matrix of the data and t_i the theoretical predictions. It is important to remark that also for the growth rate data we put practically no prior constraint on Ω_{m0} (i.e. uniform prior between 0.05 and 0.95), since Ω_{m0} will be already severely constrained by SN data.

We collected all the current independent published estimates of $f\sigma_8(z)$ obtained with the redshift space distortion method from 2dFGS (Percival et al. 2004), 6dFGS (Beutler et al. 2012), LRG (Samushia et al. 2012; Chuang & Wang 2013), BOSS (Tojeiro et al. 2012), CMASS (Chuang et al. 2013; Samushia et al. 2014), WiggleZ (Blake et al. 2012) and VIPERS (de la Torre et al. 2013) (see also Macaulay, Wehus & Eriksen 2013; Beutler et al. 2014; More et al. 2014; Reid et al. 2014). All together they cover the redshift interval [0.07, 0.8]. In some cases the correlation coefficient between two samples has been estimated in Macaulay et al. (2013) and included in our analysis. In the following, we will refer to this data with redshift space distortion ('RSD').

It is important to note that the RSD data are in principle partially degenerated with the Alcock–Paczyński (AP) effect (Alcock & Paczyński 1979), which is the fact that spherical objects do not appear spherical to observers if the wrong cosmology is assumed. One way to take the AP effect into account is to marginalize over the AP parameters, which generally enlarges the error bars but remove possible biases. All the data we use (listed above) do this either explicitly or implicitly.

We also estimated the accuracy of the estimation of $f\sigma_8(z)$ obtained from redshift distortions in the redshift range [0.5, 2.1] in a future survey that approximates the *Euclid* mission (Laureijs et al. 2011; Amendola et al. 2013); this has been obtained in Amendola et al. (2014), to which we refer for all the exact specifications. In the following we will refer to this data with '*Euclid*'. Needless to say, the *Euclid* mission will provide much more cosmological information, but here we will utilize only RSD data because in a ΛCDM background they depend only on Ω_{m0}, γ and σ_8.

To sum up, we will focus our study on the following data combinations:

(i) *current*: the JLA SN catalouge with the *Chandra* low-redshift cluster sample (see Fig. 3) and the current RSD data (see Fig. 4),
(ii) *future*: the LSST (and also *WFIRST*) SN catalouge with *Euclid*-like forecast data (see Fig. 6).

4 CONSTRAINTS ON f_g AND σ_8

For simplicity and numerical convenience we will fix all the cosmological parameters to the *Planck* 2013 best-fitting values (see Section 2.2). Only σ_8, Ω_{m0} and the growth-rate parameters will be let free. This is justified by the fact that lensing depends weakly on parameters other than these (Marra et al. 2013). In fact, Ω_{m0} is already presently constrained at the 12 per cent level by SN data (Betoule et al. 2014) and will be much more so by future LSST SN data (the exact precision cannot be easily forecast as it will likely be systematics dominated) and by *Euclid*. Thus, whenever we use LSST data it is in practice irrelevant whether we marginalize over or fix the tightly constrained Ω_{m0}. Moreover, as shown by Rapetti et al. (2010), Ω_{m0} is not strongly correlated with γ. In other words, the γ-parametrization allows to probe departures from GR, independently from the modelling of the background (Ω_{m0} in this case). Nevertheless, in order to obtain conservative results, when using JLA data we always marginalize over Ω_{m0}.

4.1 Current constraints

The non-Gaussian lensing scatter in present SN catalouges cannot yet put significant bounds in perturbation quantities, as much more statistics is needed. Nevertheless, it is interesting to investigate the current confidence levels for at least two reasons. The first is that it

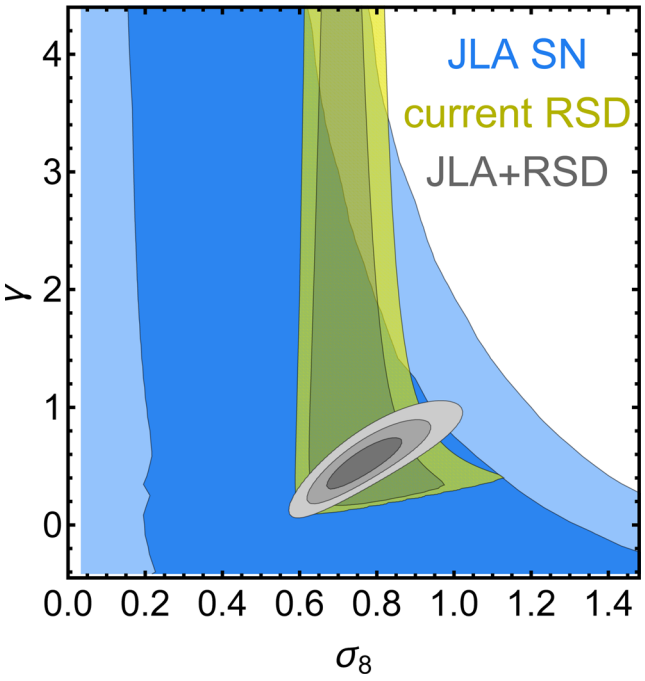

Figure 4. Similar to Fig. 3 but now combining JLA SNe with present RSD data (see Section 3.3). The combined contours are much smaller than what could be inferred by eye because the growth rate constraints depend strongly on the prior on Ω_{m0}, which present SNe already constrain quite well. As explained in the text we adopt here a very broad $0.05 < \Omega_{m0} < 0.95$ prior. The same remark holds for Fig. 6.

Table 2. One-dimensional 1σ constraints (marginalized over the remaining parameters) relative to Figs 3, 4 and 6.

	JLA+*Chandra*	JLA+RSD	LSST+*Euclid*
σ_8	$0.77^{+0.03}_{-0.04}$	$0.76^{+0.07}_{-0.06}$	0.83 ± 0.005
γ	unconstrained	$0.52^{+0.16}_{-0.13}$	0.55 ± 0.04

illustrates the improvements future probes can bring to this analysis, if systematics can be kept under control. The second is that it allows to test whether systematics are already biasing the current results.

Figs 3 and 4 show the constraints on σ_8 and γ for the combinations of JLA data with the *Chandra* low-redshift cluster sample and RSD growth rate data, respectively. The SN constraints have been marginalized over the second and third intrinsic moments, as discussed at the end of Section 3.1.1. For the growth data we assumed a flat prior corresponding to $0.05 < \Omega_{m0} < 0.95$, which effectively corresponds to $0.05 < \Omega_{m0} < \infty$ (i.e. basically we only assume the baryons density has been constrained by e.g. big bang nucleosynthesis measurements). As it can be seen, current SN data seems to be perfectly unaffected by systematics, and can already help improve the constraints obtained by either of the other two techniques alone. It is important to note, however, that the improvement in the contours comes mostly from the fact that SN constrains Ω_{m0} much better than the other techniques, while lensing currently plays only a minimal constraining role.

Marginalized constraints can be found in Table 2.

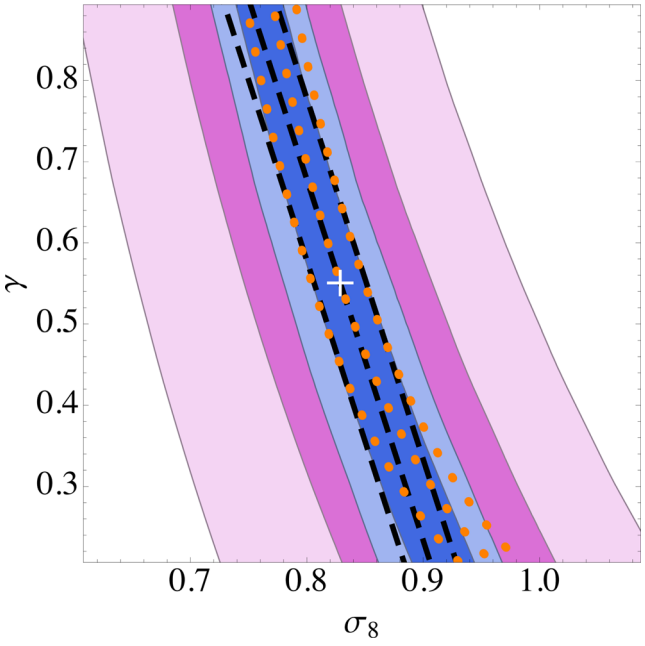

Figure 5. 1σ and 2σ marginalized constraints on γ and σ_8 using the LSST (blue contours) and *WFIRST* (orchid contours) SN catalouges of Fig. 2. Empty contours show the parametrizations for the degenerate constraints on γ and σ_8 given by equation (16) (orange dotted lines) and equation (17) (black dashed lines). The fiducial model $\{\sigma_{8,\rm fid}, \gamma_{\rm fid}\} = \{0.83, 0.55\}$ is marked with a white cross.

4.2 Future constraints

4.2.1 γ-parametrization

In Fig. 5 constraints on γ and σ_8 using synthetic catalouges from LSST and *WFIRST* are shown. These posteriors have been marginalized over the second-to-fourth intrinsic moments, but not over Ω_{m0} as LSST will tightly constrain it and results are unchanged if Ω_{m0} is simply kept fixed. As commented at the beginning of Section 4, Ω_{m0} is also not strongly correlated with γ and thus these constraints are expected to be valid even in the case that the constraints from LSST on Ω_{m0} get compromised because of systematics. *WFIRST* constraints have proven not to be competitive. In the remaining of this paper we will only use the LSST catalouge to make forecasts.

The constraints of Fig. 5 can be summarized using either of the following two parametrizations:

$$\gamma \left(\frac{\sigma_8}{\sigma_{8,\rm fid}}\right)^{\alpha} = \gamma_{\rm fid} \pm \sigma_\gamma \,, \tag{16}$$

$$\gamma - \gamma_{\rm fid}\left(1 - \frac{\sigma_8}{\sigma_{8,\rm fid}}\right)\alpha = \gamma_{\rm fid} \pm \sigma_\gamma \,, \tag{17}$$

where, in both cases, $\alpha \approx 6.7$ and $\sigma_\gamma \approx 0.1$. These parametrizations are valid near the (best fitting) fiducial model and are shown as empty contours in Fig. 5. Parametrization (17) performs better than (16) for very low values of γ. The result of equation (16) can be compared with the results of Rapetti et al. (2010), where the combination of X-ray luminosity function (XLF), $f_{\rm gas}$, SN Ia, BAO and CMB data has given the constraint $\gamma(\sigma_8/0.8)^{6.8} = 0.55^{+0.13}_{-0.10}$. This shows how future LSST constraints alone could be as competitive as all the present-day constraints (considered in Rapetti et al. 2010) combined.

Fig. 6 shows LSST and *Euclid*-like constraints on σ_8 and γ, and also the joint contours. The *Euclid*-like constraints are shown for

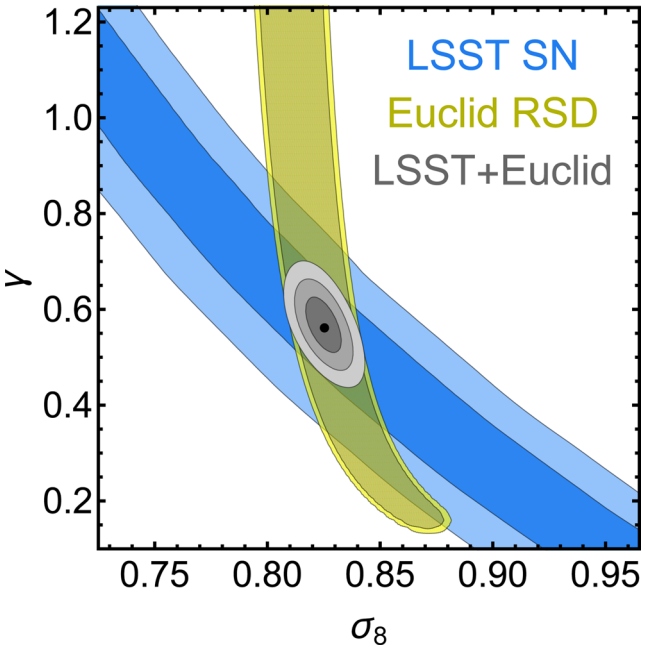

Figure 6. Similar to Fig. 4, this time forecasting future SN and growth of structure data. For the SNe we use the LSST catalouge assuming 500 000 SNe, each with a total Hubble diagram scatter of 0.15 mag; for the growth of structure, we use forecast data for a *Euclid*-like probe with a $0.05 < \Omega_{\rm m0} < 0.95$ prior. See Section 4.2.1 for more details and Table 2 for the marginalized constraints.

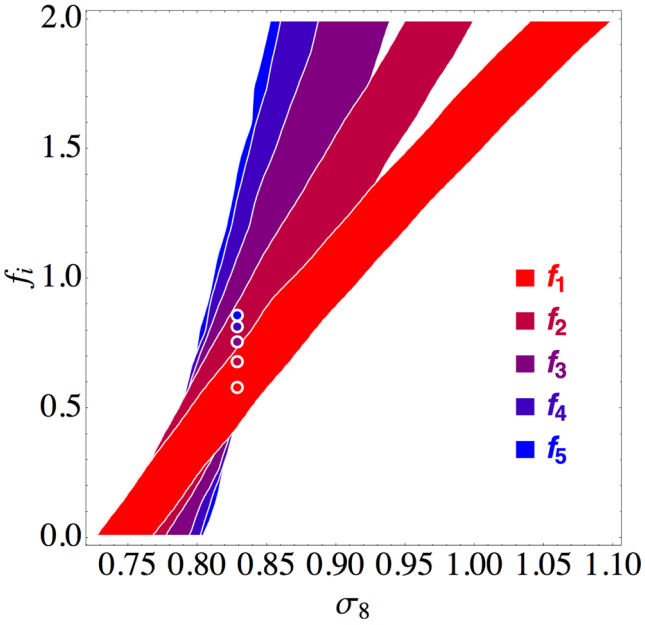

Figure 7. 1σ marginalized constraints on σ_8 and f_i of equation (5) using the LSST catalouge. The binned values of the growth rate are varied one at time, the others are assumed to take the standard values listed in Table 1. See Section 4.2.2.

the case in which the posterior is marginalized over $\Omega_{\rm m0}$ with a flat prior $0.05 < \Omega_{\rm m0} < 0.95$ (although here, RSD data do allow higher $\Omega_{\rm m0}$). Marginalized constraints can be found in Table 2. Although once again the majority of the constraining power of SN comes from the nailing down of $\Omega_{\rm m0}$, the SN lensing contours (from the higher moments) start to become competitive, and pose an important cross-check to the more standard techniques.

In fact, this plot clearly shows how – in the quest for stricter dark energy constraints – one should rely on different probes as they suffer different parameter degeneracies and can efficiently complement each other. Also, different probes are subject to different systematic uncertainties, and any new probe is obviously welcome in order to cross-check the validity of other measurements. The importance of such complementarity regarding constraints on σ_8 and γ has been exemplified by Rapetti et al. (2013) where a combination of galaxy growth, CMB and cluster growth observables was able to completely break the degeneracy.

4.2.2 f-*parametrization*

Here we forecast constraints on the binned values $f_{\bar{i}}$ of equation (5), taken one at time. Bins for which $i \neq \bar{i}$ are assumed to take the standard values listed in Table 1. Fig. 7 shows how the 68 per cent constraints (marginalized over intrinsic moments) rotate and get weaker as the corresponding redshift increases. Constraints get weaker because lensing is an integrated effect and will differ more with respect to the standard model if the change in the growth rate extends for a larger redshift range (see e.g. Fig. 1). Constraints rotate because lensing is less sensitive with respect to changes in growth rate at larger redshifts. Also, it is interesting to note that – if let free – $f_{\bar{i}}$ and $f_{\bar{j}}$ are anticorrelated. This is expected as an increase in e.g. $f_{\bar{i}}$ needs to be compensated by a decrease in $f_{\bar{j}}$ in order to have an equivalent growth of structure. As mentioned before, this analysis could have been done using a different gravity theory, and Fig. 7 also shows that SN lensing analysis can potentially be another way to test modified gravity, being more sensitive to models that predict deviation from the standard model at smaller redshifts.

These LSST constraints can be summarized using the following parametrization:

$$f_i - f_{i,\rm fid}\left(1 - \frac{\sigma_8}{\sigma_{8,\rm fid}}\right)\alpha_i = f_{i,\rm fid} \pm \sigma_i \,, \tag{18}$$

where the value of $f_{i,\rm fid}$ are given in Table 1 and the parameters α_i and σ_i by the following linear fit:

$$\alpha_i = -8.9 - 12\,\bar{z}_i \,, \tag{19}$$

$$\sigma_i = 0.12 + 0.35\,\bar{z}_i \,, \tag{20}$$

where $\bar{z}_i$ is the redshift value at the centre of the redshift bin $[z_{i-1}, z_i)$. These constraints should be valid for bins at redshifts $z \neq \bar{z}_i$ as long as the bin has a width of $\Delta z = 0.2$. As in Section 4.2.1, these constraints have been marginalized over the second-to-fourth intrinsic moments but not over $\Omega_{\rm m0}$, again because for LSST this is irrelevant.

5 CONCLUSIONS

In this paper, we studied the current and future constraints on the linear matter growth rate and on the power spectrum normalization σ_8 using SN lensing through a recently proposed technique combined with other data. The growth rate is parametrized either in the popular form $f = \Omega_{\rm m}^{\gamma}$ or as a stepwise constant function. For the present data, we included data sets taken from the JLA SN Ia catalogue, from the *Chandra* low-redshift cluster sample, and from all the available $f\sigma_8(z)$ redshift-distortion data. The final results, summarized in Table 2, show that σ_8 can be constrained by

the combined data sets (in particular by JLA and RSD) to within 10 per cent roughly, while γ is only poorly constrained to within 30 per cent (all errors at 1σ). Current SN data alone put only very broad constraints on γ, σ_8 and the results are driven by the other data sets.

For the future constraints we show that, with 500 000 LSST SNe with average total dispersion of 0.15 mag, the constraints on γ, σ_8 will lie on a band parametrized by equation (16) or (17), see Fig. 6. It is worth stressing that future LSST constraints alone can potentially be as competitive as all present-day constraints together. When combined with *Euclid*-like results on $f\sigma_8(z)$ from redshift distortions, the parameters will be constrained to within 0.6 per cent and 7 per cent on σ_8 and γ, respectively (see Table 2). We also explored the constraints on a general, step-wise parametrization of the growth rate f.

The three Figs 3, 4 and 6 nicely show the twofold beneficial effect of SN lensing analysis: at the background level (the first moment of the lensing PDF) it breaks the degeneracy on Ω_{m0} and σ_8 – this is why we obtain better results than what would naively be inferred by eye – and at the perturbation level (the higher moments) it breaks the degeneracy on γ and σ_8.

The main interest in this method based on SN lensing is that it exploits an effect completely different from the standard ones based on clusters abundances, galaxy clustering, weak-lensing and strong-lensing abundances, and therefore subject to different systematics. An additional bonus of our method is that a deviation from the parameters that fit other probes could signal for instance a redshift dependence of the SN magnitude central moments, which could then be related to redshift-dependent physics of SN light curves.

ACKNOWLEDGEMENTS

It is a pleasure to thank Chia-Hsun Chuang and David Rapetti for fruitful discussions. LA acknowledges support from DFG through the TRR33 programme 'The Dark Universe'. TC is grateful to Brazilian research agency CAPES. VM was supported during part of this project by a Science Without Borders fellowship from the Brazilian Foundation for the Coordination of Improvement of Higher Education Personnel (CAPES). MQ is grateful to Brazilian research agencies CNPq and FAPERJ for support.

REFERENCES

Abell P. A. et al., 2009, preprint (arXiv:0912.0201)
Alcock C., Paczynski B., 1979, Nature, 281, 358
Amendola L., Tsujikawa S., 2010, Dark Energy: Theory and Observations. Cambridge Univ. Press, Cambridge
Amendola L. et al., 2013, Living Rev. Relativ.., 16, 6
Amendola L., Fogli S., Guarnizo A., Kunz M., Vollmer A., 2014, Phys. Rev. D, 89, 063538
Astier P. et al., 2014, A&A, 572, A80
Bartelmann M., Schneider P., 2001, Phys. Rep., 340, 291
Ben-Dayan I., Gasperini M., Marozzi G., Nugier F., Veneziano G., 2013, J. Cosmol. Astropart. Phys., 1306, 002
Bernardeau F., Van Waerbeke L., Mellier Y., 1997, A&A, 322, 1
Betoule M. et al., 2013, A&A, 552, 124
Betoule M. et al., 2014, A&A, 568, A22
Beutler F. et al., 2012, MNRAS, 423, 3430
Beutler F. et al., 2014, MNRAS, 443, 1065
Blake C. et al., 2012, MNRAS, 425, 405
Castro T., Quartin M., 2014, MNRAS, 443, L6
Chuang C.-H., Wang Y., 2013, MNRAS, 435, 255
Chuang C.-H. et al., 2013, preprint (arXiv:1312.4889)
Conley A. et al., 2011, ApJS, 192, 1
Courtin J., Rasera Y., Alimi J.-M., Corasaniti P.-S., Boucher V., Füzfa A., 2011, MNRAS, 410, 1911
de la Torre S. et al., 2013, A&A, 557, A54
Dodelson S., Vallinotto A., 2006, Phys. Rev. D, 74, 063515
Green J. et al., 2012, preprint (arXiv:1208.4012)
Hamana T., Futamase T., 2000, ApJ, 534, 29
Jönsson J., Dahlén T., Hook I., Goobar A., Mörtsell E., 2010a, MNRAS, 402, 526
Jönsson J. et al., 2010b, MNRAS, 405, 535
Kainulainen K., Marra V., 2009, Phys. Rev. D, 80, 123020
Kainulainen K., Marra V., 2011a, Phys. Rev. D, 83, 023009
Kainulainen K., Marra V., 2011b, Phys. Rev. D, 84, 063004
Kessler R. et al., 2009, ApJS, 185, 32
Kronborg T. et al., 2010, A&A, 514, A44
Laureijs R. et al., 2011, preprint (arXiv:1110.3193)
Macaulay E., Wehus I. K., Eriksen H. K., 2013, Phys. Rev. Lett., 111, 161301
Marra V., Quartin M., Amendola L., 2013, Phys. Rev. D, 88, 063004
More S., Miyatake H., Mandelbaum R., Takada M., Spergel D., Brownstein J., Schneider D. P., 2014, preprint (arXiv:1407.1856)
Percival W. J. et al., 2004, MNRAS, 353, 1201
Planck Collaboration XVI , 2014, A&A, 571, A16
Quartin M., Marra V., Amendola L., 2014, Phys. Rev. D, 89, 023009
Rapetti D., Allen S. W., Mantz A., Ebeling H., 2010, MNRAS, 406, 1796
Rapetti D., Blake C., Allen S. W., Mantz A., Parkinson D., Beutler F., 2013, MNRAS, 432, 973
Reid B. A., Seo H.-J., Leauthaud A., Tinker J. L., White M., 2014, MNRAS, 444, 476
Samushia L., Percival W. J., Raccanelli A., 2012, MNRAS, 420, 2102
Samushia L. et al., 2014, MNRAS, 439, 3504
Scolnic D. et al., 2014, ApJ, 795, 45
Sheth R. K., Tormen G., 1999, MNRAS, 308, 119
Tojeiro R. et al., 2012, MNRAS, 424, 2339
Valageas P., 2000, A&A, 356, 771
Vikhlinin A. et al., 2009, ApJ, 692, 1060
Zhao D., Jing Y., Mo H., Boerner G., 2009, ApJ, 707, 354

APPENDIX A: FITTING FUNCTIONS

Here we will give simple analytical fitting functions for the second-to-fourth central lensing moments $\mu_{2-4,\,\mathrm{lens}}$ as a function of $\{z, \sigma_8, \gamma\}$, which are valid within the domain:

$$0 \le z \le 1.2\,,$$
$$0.6 \le \sigma_8 \le 1,$$
$$0 \le \gamma \le 1.1.$$

All the other cosmological parameters have been fixed to the *Planck* 2013 best-fitting values (see Section 2.2). Using magnitudes, the fitting formulae are

$$\sigma_{\mathrm{lens}}(z, \sigma_8, \gamma) = \sigma_8 z(0.0164\gamma + 0.0145z + 0.0396)\,, \quad \text{(A1)}$$

$$\mu^{1/3}_{3,\mathrm{lens}}(z, \sigma_8, \gamma) = \sigma_8 z(0.0283\gamma - 0.006\,96z + 0.0861)\,, \quad \text{(A2)}$$

$$\mu^{1/4}_{4,\mathrm{lens}}(z, \sigma_8, \gamma) = \sigma_8 z(0.0393\gamma - 0.0344z + 0.153)\,. \quad \text{(A3)}$$

In the entire domain of validity, the average rms error is 0.0012, 0.0017 and 0.0021 for $\mu_{2-4,\,\mathrm{lens}}$, respectively, which is roughly 3 per cent for all three moments.

This paper has been typeset from a TEX/LATEX file prepared by the author.